Journal of Integrative Neuroscience

Original Research

The anti-aging effect of velvet antler polypeptide is dependent on modulation of the gut microbiota and regulation of the PPARα/APOE4 pathway

Xiaoran Liu[1,†], Qing Yang[1,†], Hui Li[2], Xingcheng Lan[1], Mo Kan[1], Jianan Lin[1], Jifeng Wang[1], Zhuang Zhang[1], Sitong Ming[1], Zhen Li[1], Yaxin Liu[1], Yanhong Zhang[1], Qihang Pang[1], Song Gao[1], Na Li[1,*]

[1]*Jilin Ginseng Academy, Changchun University of Chinese Medicine, 130117 Changchun, Jilin, China*

[2]*Department of General Surgery, Qian Wei Hospital of Jilin Province, 130117 Changchun, Jilin, China*

*Correspondence: lhaln@hotmail.com (Na Li)
† These authors contributed equally.

DOI:10.31083/j.jin2003061

Submitted: 14 May 2021 Revised: 25 June 2021 Accepted: 7 July 2021 Published: 30 September 2021

We investigated the anti-aging effects of velvet antler polypeptide on D-galactose (D-gal)-induced aging mice. D-gal-induced aging mice were established and randomly divided into five groups, the control, model, vitamin E (VE), velvet antler polypeptide low-dose and velvet antler polypeptide high-dose groups. The Morris water maze test was used to evaluate the learning and memory abilities of aging mice. Hippocampal neurons were observed via hematoxylin-eosin staining and transmission electron microscopy. Biochemical methods were used to detect the activities of superoxide dismutase, malonaldehyde and other enzymes and evaluate the influence of velvet antler polypeptide on the antioxidant capacity of aging mice. Using 16S rRNA gene sequencing and meristem technology, we assessed the effect of velvet antler polypeptide on aging mice's intestinal flora and fatty acid metabolism. The experimental results showed that velvet antler polypeptide could significantly improve aging mice's learning and cognitive abilities, increase the activities of superoxide dismutase, glutathione peroxidase, and catalase in the serum decrease the malonaldehyde content. Intestinal microecological analysis showed that velvet antler polypeptide could significantly increase the beneficial bacterial genus *Lactobacillus* abundance. Western blot analysis further demonstrated that velvet antler polypeptide could promote fatty acid metabolism by activating peroxisome proliferator-activated receptor α (PPARα) and upregulating the expression of the downstream enzymes carnitine-palmitoyl transferase-1 A and acyl-CoA oxidase 1 while downregulating that of apolipoprotein E4 (APOE4), thereby reducing fatty acid accumulation and increasing adenosine-triphosphate (ATP) production. Therefore, velvet antler polypeptide improves the intestinal microecology and activates the PPARα/APOE4 pathway to regulate fatty acid metabolism.

Keywords

Velvet antler polypeptide; D-galactose; Aging; Intestinal microecology; Learning; Cognitive impairment; PPARα/APOE4 pathway; Microbiota

1. Introduction

Velvet antler polypeptide (VAP) accounts for 50–60% of the wet weight of velvet antler and is one of its primary active ingredients [1]. VAP is rich in proteins, amino acids, phospholipids, cholesterol, and calcium ions and exerts various health-promoting effects, with antioxidant [2], osteoporosis resistance [3], and immune regulation [4] effects having been reported. To better understand the role of VAP in the prevention and treatment of neurodegenerative diseases, previous research by our research group also confirmed that VAP could reduce the levels of the glucocorticoid receptor, mineralocorticoid receptor and corticotropin-releasing hormone. The effects of VAP on the thalamus-pituitary-adrenal axis and its ability to inhibit neuronal apoptosis have also been observed [5].

Brain aging is a natural physiological process characterized by oxidative stress (OS), the accumulation of oxidative damage molecules, and changes in the structure and function of neurons, ultimately leading to cognitive decline and memory loss [6]. Among these factors, OS is considered the primary cause of aging-associated neurodegenerative diseases [7]. When the body is subjected to harmful stimuli, there is an imbalance between the generation and removal of free radicals, resulting in an increase in free radicals to a level that exceeds the antioxidant capacity in the body. Notably, excessive free radicals are cytotoxic, causing direct damage to the central nervous system [8, 9]. The human brain accounts for only 2–3% of the human body weight. Still, the central nervous system (CNS) accounts for 20% of the total oxygen supply of the human body. Therefore, the content of neuronal free radicals in the CNS is considerable, presenting a high risk of OS [10].

The human gut microbiota, which comprises more than 100 species, comprises approximately 10-fold more bacteria than human cells [11]. Firmicutes is the most abundant species within the human gut microbiota, accounting for 60%

of total bacteria, followed by Bacteroidetes (15%) and other components that account for a small proportion. The gut microbiota is in a state of dynamic balance with the human body, and intestinal microbes have an important role in human metabolism, endocrine function, and immune regulation. Therefore, when the gut microbiota structure is disturbed, neurodegenerative diseases, cardiovascular diseases, and obesity may occur [12]. Changes in the quantity and diversity of intestinal microorganisms can also affect the enteric and central nervous systems. These interactions are known as the microbiota-gut-brain axis, which is important for body function [13, 14]. Although changes in gut microbiota profiles do not necessarily affect health, the loss of diversity in the core microbiota is associated with decreased cognitive function and memory [15]. Indeed, with increasing age, the changes in bacterial flora are primarily characterized by decreases in diversity, probiotics, facultative anaerobes, and total short-chain fatty acids [16].

Although numerous studies have confirmed that VAP-associated antioxidant and anti-aging effects attenuate aging, the exact mechanism underlying this activity has remained unclear. Therefore, in the present work, the anti-aging effect of VAP was evaluated *in vivo* in mice via the Morris water maze (MWM) test, biochemical analysis, hematoxylin-eosin (H&E) staining, and transmission electron microscopy (TEM). Furthermore, we evaluated the changes in the intestinal microecology in aging mouse models treated with VAP using 16S ribosomal RNA (rRNA) gene sequencing technology. Our goal was to elucidate the mechanism of VAP activity in the context of aging and provide a theoretical basis for the development of new anti-aging therapeutic approaches.

2. Materials and methods

2.1 Experimental materials

VAP was provided by the Molecular Pharmacology Laboratory, Changchun University of Chinese Medicine. D-galactose (D-gal) and VE (purity >90%) were purchased from Shanghai Yuanye Biotechnology Co., Ltd. (Shanghai, China). Commercial superoxide dismutase (SOD), malonaldehyde (MDA), catalase (CAT), and glutathione peroxidase (GSH-Px) kits were purchased from Nanjing Jiancheng Technology Co., Ltd. (Nanjing, China). All chemicals and reagents were of analytical grade.

The Morris water maze (MWM) video tracking and analysis system were purchased from Chengdu Taimeng Technology Co., Ltd. (Chengdu, China). A transmission electron microscope was purchased from Tecnai Corporation (Hillsboro, OR, USA). The high-throughput sequencing platform (MiSeq PE300) was provided by Illumina (San Diego, CA, USA).

2.2 Animal experiments

Sixty healthy ICR mice (SPF grade, half male and half female, weighing 22–26 g) were purchased from Changchun Yisi Laboratory Animal Technology Co., Ltd. (certificate No. SCXK(Ji) -2018-0007). The mice were raised in separate cages under 12 h light/dark cycles and a standard temperature (22 ± 2 °C), with food and water provided ad libitum. All mice were adapted to these conditions for at least one week before the experiments commenced. All mice were divided into five groups, the control, model, vitamin E (VE), VAP low-dose (VAP1) and VAP high-dose (VAP2) groups. The VE, VAP1, and VAP2 groups were administered VE (100 mg/kg), VAP (200 mg/kg) and VAP (400 mg/kg), respectively, for 10 days, while the control and model groups received distilled water (the same volume and via the same intragastric route). Starting on the 11th day, the control group was subcutaneously injected with normal saline. D-gal (1000 mg/kg) was subcutaneously injected into the back of the neck of the mice in the other groups, and the model administration was continued for 60 days.

2.3 Morris water maze

The MWM test was performed 1 h after D-gal administration on day 57. Briefly, a platform was placed in the middle of the water maze. Water was added to the platform until it exceeded 1 cm and was maintained at approximately 25 °C. The mice were trained continuously for 1 week, and the MWM test was formally performed per the water maze standard operating procedure. Before the official start of the experiment, titanium dioxide was added to the water so that the mice could not perceive the specific position of the platform. The heads of the mice were dyed yellow to track and collect data. The Morris water maze video-tracking analysis software recorded the swimming path of the mice, the percentage of residence time in the middle ring, and the percentage of the middle ring movement distance.

2.4 H&E staining

The whole brains of mice were fixed in 4% paraformaldehyde solution and embedded in paraffin. After 24 h, the brain tissues were sectioned, deparaffinized, rehydrated and stained with H&E. The sections were then observed under an optical microscope to record the pathological changes.

2.5 TEM

After perfusion, the hippocampal tissues were severed, fixed with 2% paraformaldehyde and 2.5% glutaraldehyde phosphate buffer solution, dehydrated using an alcohol gradient, cleaned with ethoxypropane, embedded, sliced, and stained with uranyl acetate and lead citrate. The ultrastructure of hippocampal neurons was observed under a transmission electron microscope.

2.6 Biochemical analyses

Mouse blood samples were collected and centrifuged at 3000 rpm for 15 min at 4 °C, after which the supernatant was collected. The serum MDA content and SOD, GSH-Px, and CAT activity determination were all carried out in accordance with the kit instructions.

2.7 Microbiota profiling of fecal samples

Total DNA was extracted from fecal samples and used as a template to PCR amplify the V3–V4 region of the bacterial 16S rRNA gene. The raw dataset is deposited in NCBI BioProject PRJNA731623 under the BioSample accession numbers SAMN19291644 to SAMN19291668. The PCR products were quantitatively analyzed, and 16S rRNA gene sequencing was performed using an Illumina MiSeq platform (Illumina, San Diego, USA). The raw data is based on the minimum overlap length of 10 bp, with a maximum allowable mismatch ratio in the overlap area of 0.2 (default). The reads of each sample were spliced, and tags with lengths less than 75% of the tag length after quality control were filtered. The chimeras (that is, if the two parents have a sequence that is more than 80% similar to the query sequence, then the query is judged to be a chimera) were removed to obtain high-quality tag sequences. Usearch software (Sonoma, USA) [17] was used to cluster tags at a 97% similarity level, classify operational taxonomic units (OTUs), obtain species classification based on OTU sequence composition, and plot sample dilution [18] and Shannon index curves. PICRUSt (Halifax, CAN) [19] was used to determine the functional gene composition of each sample via comparison of the species composition information according to 16S rRNA gene sequencing results. In this way, functional differences between different samples or groups could be determined. The abundances, pathways, EC information, and OTU abundances in the context of each functional category were obtained using the Kyoto Encyclopedia of Genes and Genomes [20] database.

2.8 Western blotting

Total protein was extracted from brain tissue, and the Coomassie brilliant blue method was used to assess the protein concentration. Then, after SDS-PAGE electrophoresis, the proteins have transferred to the membrane, which was then incubated with primary antibodies against target proteins apolipoprotein E (APOE4), acyl-CoA oxidase 1 (ACOX1), peroxisome proliferator-activated receptor α (PPARα), carnitine-palmitoyl transferase-1 A (CPT1A), and glyceraldehyde-3-phosphate dehydrogenase(GAPDH) overnight at 4 °C. Subsequently, the membrane was washed and then incubated with a secondary antibody at room temperature for 1 h. After washing the membrane with Tris-buffered saline and Tween 20 (TBST), enhanced chemiluminescent (ECL) solution was added. A fully automatic gel imaging system (Aplegen, Pleasanton, USA) is used for scanning photography.

2.9 Detection of free fatty acid(FFA) levels in brain tissue

Mouse brain tissues were collected, and an appropriate amount of normal saline was added. Then, the samples were centrifuged at 4 °C at 3000 rpm for 10 min, and the supernatants were collected. The FFA levels in brain tissues were determined in accordance with the kit instructions.

2.10 Detection of ATP content in brain tissue

Mouse brain tissues were collected and lysed at a brain tissue: lysis buffer ratio of 1:5. Then, the samples were centrifuged at 12,000× g at 4 °C for 5 min, and the supernatants were collected. The ATP contents in brain tissues were determined in accordance with the kit instructions.

2.11 Statistical analysis

SPSS 19.0 (Chicago, IL, USA) was used for data analysis. The results are expressed as the mean ± standard deviation ($\overline{x} \pm s$). The student's *t*-test was used to compare groups, and differences were considered significant at $P < 0.05$ or $P < 0.01$.

3. Results

3.1 Improvement of cognition, learning, and memory in aging mice treated with VAP

The MWM test relies on the survival instinct of animals to find the escape platform and involves searching for a memory-related spatial position. Fig. 1 shows representative tracks of mice administered the MWM test on the last day. The mouse behavior trajectory diagram of the model group was more complicated and irregular, and the mice did not find the platform. Of note, the behavior trajectory diagram of the mice in the VAP1 and VAP2 groups was simple, and a platform was found. Compared with the Control group, the percentage of retention time in the middle ring and the percentage of the distance moved by the middle ring in the Model group were significantly reduced ($P < 0.01$). Compared with the Model group, the percentage of retention time in the middle ring and the percentage of the distance moved by the middle ring were significantly increased in the VE, VAP1 and VAP2 groups ($P < 0.05$, $P < 0.01$). These findings indicate that the administration of VAP improved the cognitive ability of D-gal-induced aging mice.

3.2 Protective effect of VAP on hippocampal neurons in aging mice

H&E staining was used to observe the pathological morphology of brain tissues in aging mice to explore whether VAP could improve D-gal-induced neuronal pathological damage (Fig. 2A). The CA1 cells in the hippocampi from the control group were abundant, with normal cell structure, complete morphology, and obvious nuclei. In contrast, the number of CA1 cells in hippocampi from the model group decreased and showed irregular morphology, with no obvious nucleoli observed under the microscope. The neurons in the CA1 area of hippocampi were relatively normal, and nuclear shrinkage was reduced in the VE group compared to the model group. Remarkably, the CA1 area in hippocampi from the VAP1 and VAP2 groups was significantly different from that observed in the model group and similar to that of the control group. The structure was relatively normal, the cells were closely arranged and regular, and the morphology was complete.

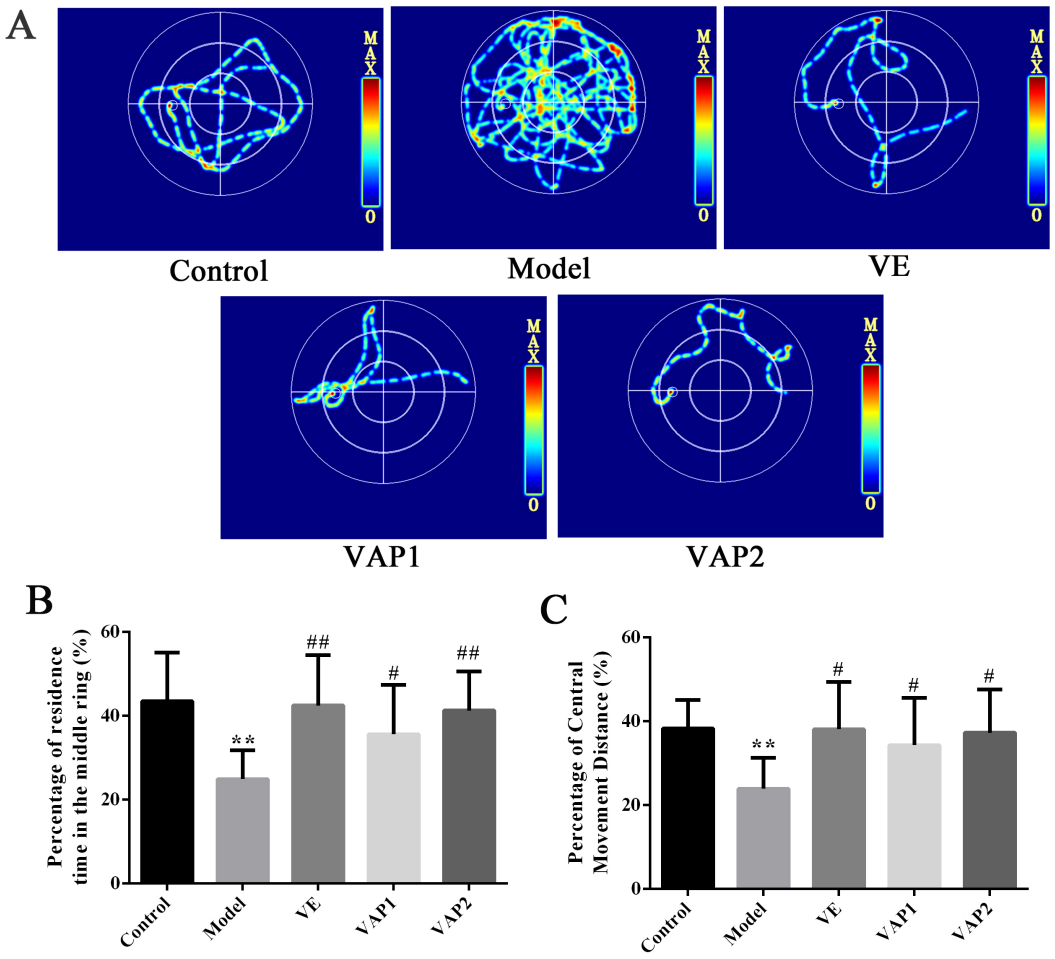

Fig. 1. MWM testing to evaluate the influence of VAP on the neurological function and behaviors of aging mice (n = 8). (A) Behavioral route of mice in each group. (B,C) Percentage of residence time in the Middle ring and Percentage of Central Movement Distance. Significant differences are denoted as follows: compared with the control group, $^{*}P < 0.05$, $^{**}P < 0.01$; compared with the model group, $^{\#}P < 0.05$, $^{\#\#}P < 0.01$.

TEM was further used to observe the ultrastructure of hippocampal neurons in aging mice and to understand whether the reversal effect of VAP on the decline in learning and memory was associated with regulating neuron microstructure in the brain (Fig. 2B). The hippocampal neurons showed an intact morphology, uniform chromatin distribution, and abundant organelles in the cytoplasm in the control group. At high magnification, the mitochondria were elliptical, with a clear double outer membrane and intact cristae. In contrast, the neurons in the hippocampal region of the model group were abnormal; early apoptotic changes such as chromatin condensation were observed; lipofuscin corpuscles were more frequent; the synaptic structure was unclear; lipid droplets were scattered, and vesicle-like expansion of the Golgi complex and reduced rough endoplasmic reticulum were detected. Remarkably, compared to the model group, the VAP1 and VAP2 groups had hippocampal neurons that tended to be normal in structure and morphology, with smooth nuclear membranes, normal nucleoli, and abundant organelles. Notably, more synapses were observed, the synaptic vesicles in the anterior membrane did not have abnormal aggregation, the morphology of the intracytoplasmic Golgi body and mitochondria was normal, and lipofuscin was rare.

3.3 Effects of VAP on oxidative damage-related enzymes

A negative effect of OS is the production of free radicals in the body, one of the primary causes of aging and disease (Fig. 3). Compared to the control group, the activities of SOD, CAT, and GSH-Px in the serum of D-gal-administered model mice were significantly decreased ($P < 0.01$, $P < 0.05$), and the MDA content was significantly increased ($P < 0.05$), indicating successful modeling. Compared to the model group, the activities of SOD, CAT and GSH-Px in the VE group were significantly increased ($P < 0.01$, $P < 0.05$). Compared to the model group, the activities of SOD and GSH-Px in the VAP1 group were significantly increased ($P < 0.05$, $P < 0.01$). In contrast, the CAT was slightly increased but was not significantly different. Compared to the model group, the activities of SOD, CAT and GSH-Px in the VAP2 group were significantly increased ($P < 0.05$, $P < 0.01$). Compared to the model group, the serum

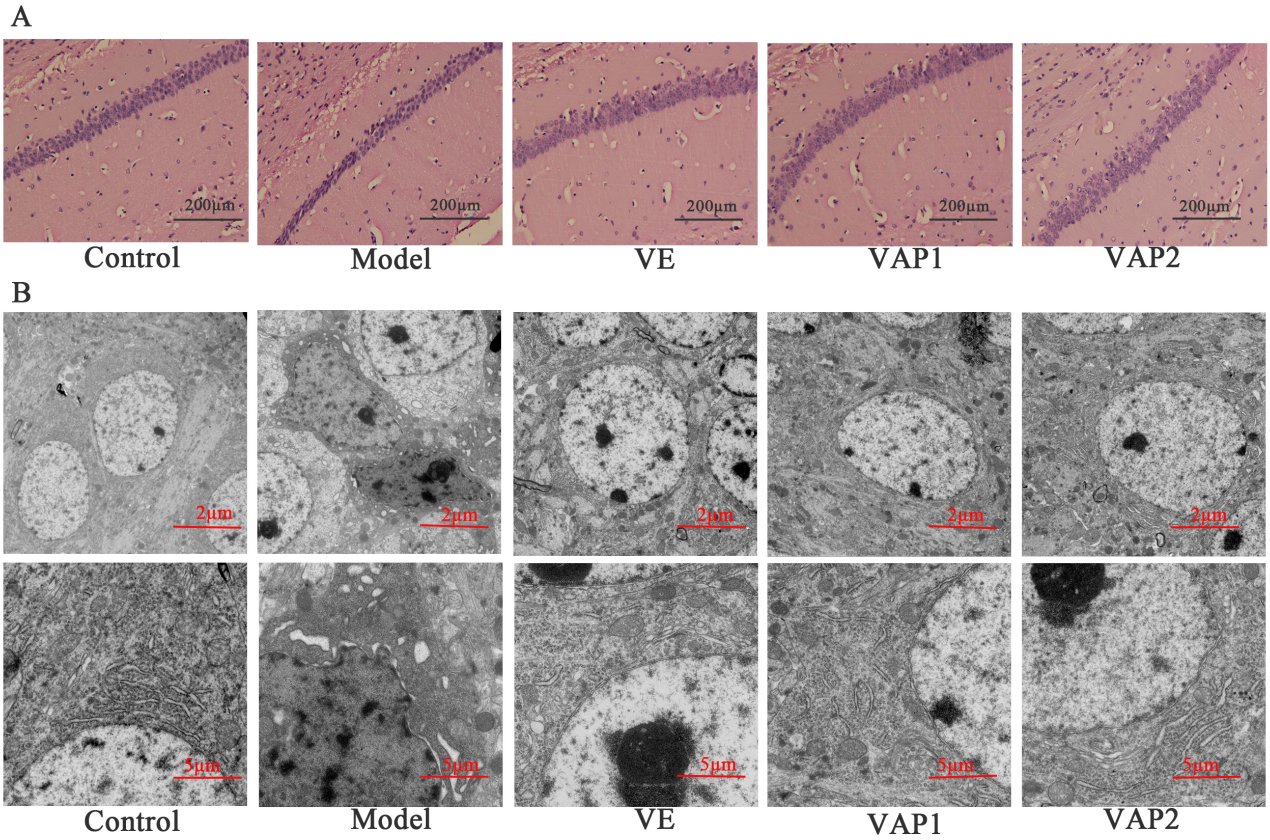

Fig. 2. Effects of VAP on the morphology of neurons in the hippocampal CA1 region in aging mice (n = 3). (A) H&E staining of the hippocampal sections of mice from each group. Scale bars = 200 μm. (B) TEM analysis of the hippocampal ultrastructure. Scale bars = 2 and 5 μm, respectively.

MDA contents of mice in the VAP1 and VAP2 groups were significantly reduced ($P < 0.05$). The above results indicate that the anti-aging effect of VAP is related to enhancing the activity of serum antioxidant enzymes in aging mice and reducing lipid peroxidation.

3.4 Effects of VAP on the composition and diversity of the gut microbiota in mice

The 16S rRNA gene sequencing results yielded 1,999,460 PE Reads, and after filtering and removing chimeras, 1,776,708 effective tags were obtained. The average sequence lengths of the samples in the control, model, VE, VAP1, and VAP2 groups were 417.2, 416.2, 418.2, 421.0, and 420.4 bp, respectively. The ratio of reads with a Phred quality score over 30 (Q30) ranged from 94.15 to 95.71%.

Subsequently, we determined the gut microbiota composition using the 16S rRNA gene reads. The tags obtained by high-throughput sequencing were clustered at a similarity level of 97%, and a Venn diagram was generated (Fig. 4A). Each group had 490 OTUs, and there were essentially no specific OTUs per group. To verify whether the sequencing depth met species identification requirements, we plotted Shannon and rarefaction curves for all samples (Fig. 4B,C). Both curves in all samples were close to the saturation plateau, revealing a high coverage (99%). These data suggest that the vast majority of the microbial diversity information in the samples was extracted and that the bacterial community structure and diversity could be accurately determined.

Alpha diversity reflects species abundance (richness) and species diversity. Shannon and Simpson indexes are used to measure species diversity and are affected by the abundance of species in the sample community and the evenness of species (community evenness). The larger the Shannon index value, the smaller the Simpson index value, indicating that the species diversity of the sample is higher [21]. The results presented in Fig. 4D show no significant differences in the Shannon index values of the mouse flora between the groups.

Compared with the control group, the Simpson index value of the model group has no significant difference. No significant difference was observed between the model group and each treatment group. These results show no significant difference in the diversity of the intestinal flora of mice between the groups.

PCA was performed on the mouse intestinal flora (Fig. 4E), where PC1 and PC2 are the two characteristic values that cause the greatest difference between samples. The results showed that 32.94 and 19.74% of the degree of influ-

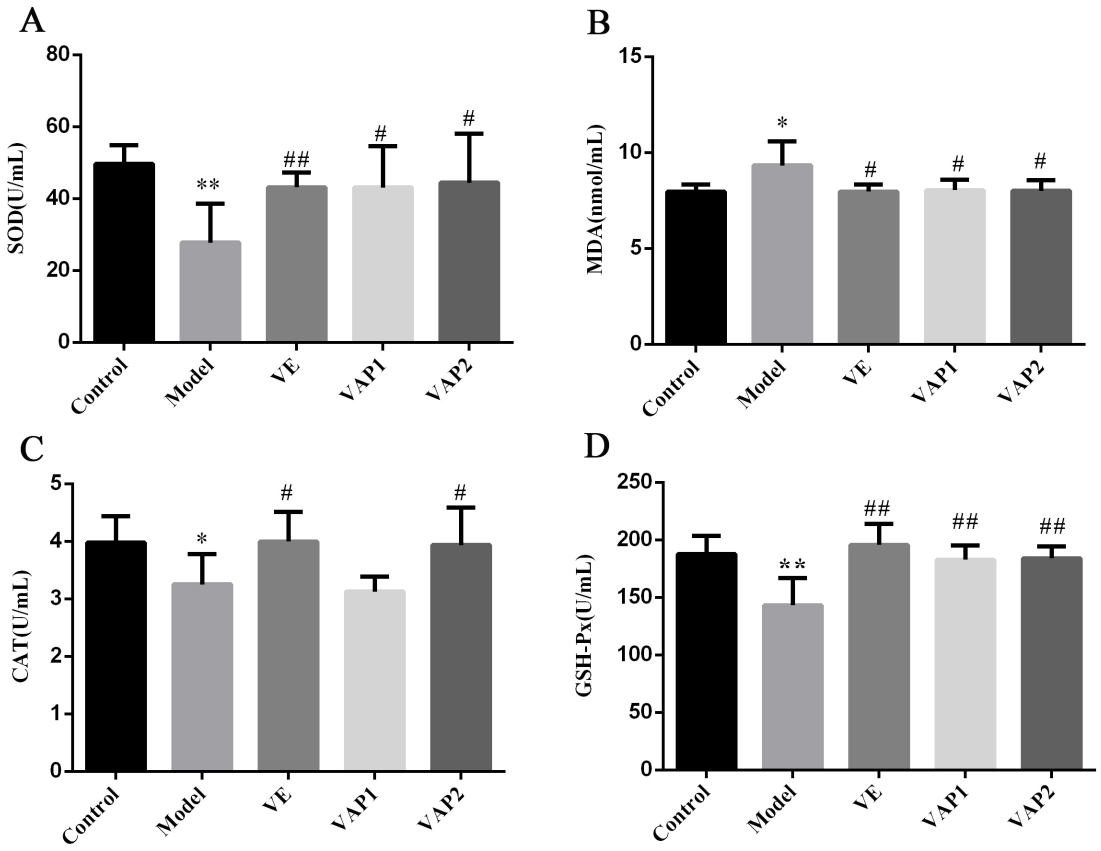

Fig. 3. Effects of VAP on the levels of SOD (A), MDA (B), CAT (C), and GSH-Px (D) in the serum of aging mice (n = 8). Significant differences are denoted as follows: compared to the control group, $^{*}P < 0.05$, $^{**}P < 0.01$; compared to the model group, $^{\#}P < 0.05$, $^{\#\#}P < 0.01$.

ence was accounted for by PC1 and PC2, respectively. The farther the points are, the greater the difference. The five groups of samples clustered into three categories, with the model group samples distributed in the upper left corner of the figure, far away from the other groups. The control, VE and VAP2 groups showed more overlaps, and the three groups of samples were close together. The upper middle of Fig. 4E shows that after VAP intervention, the similarity of the intestinal flora of the VAP2 group of mice to that of the control mice was improved.

The differences in the abundances of bacteria in the control model, VE, VAP1, and VAP2 groups were evaluated for the top 20 genera (Fig. 4F). The abundances of *Lachnospiraceae_NK4A136_group* and *Lactobacillus* were different between the control and model animals, where the abundance of *Lactobacillus* in the model group was significantly decreased. In contrast, the abundances of the remaining genera were significantly increased. Notably, *Lactobacillus* members are probiotics with anti-aging and anti-inflammatory effects [22, 23]. Therefore, these results were not surprising. Remarkably, the abundance of *Lactobacillus* was significantly increased in the VAP1 and VAP2 groups compared to the model group, suggesting that VAP may increase the content of beneficial bacteria in the gut, preventing aging.

3.5 16S rRNA gene functional prediction analysis

Using KEGG pathway analysis, differences in the metabolic pathways (functional genes) in microbial communities from the different groups were investigated. Pathways with an average abundance greater than 0.1% were selected according to the 16S rRNA gene functional prediction results. Moreover, pathways with a significant impact on the differences between groups were evaluated through random forest analysis (Fig. 5). Through KEGG analysis, the following five pathways with a significant influence on the difference between the groups were identified: ko00310 (lysine degradation), ko00071 (fatty acid degradation), ko00300 (lysine biosynthesis), ko00920 (sulfur metabolism), and ko00280 (valine, leucine, and isoleucine degradation). Notably, the value of ko00071 (fatty acid degradation) ranked second but had a greater impact on each group.

According to the predicted gut microbiota functions, we speculated that the aging cognitive impairment caused by D-gal might be related to abnormal fatty acid metabolism *in vivo*.

3.6 Influence of VAP on the fatty acid metabolism pathway

According to the 16S rRNA gene functional prediction results, we speculated that D-gal-induced aging and the consequent cognitive impairment might be associated with abnormal fatty acid metabolism. Based on this hypothesis, we

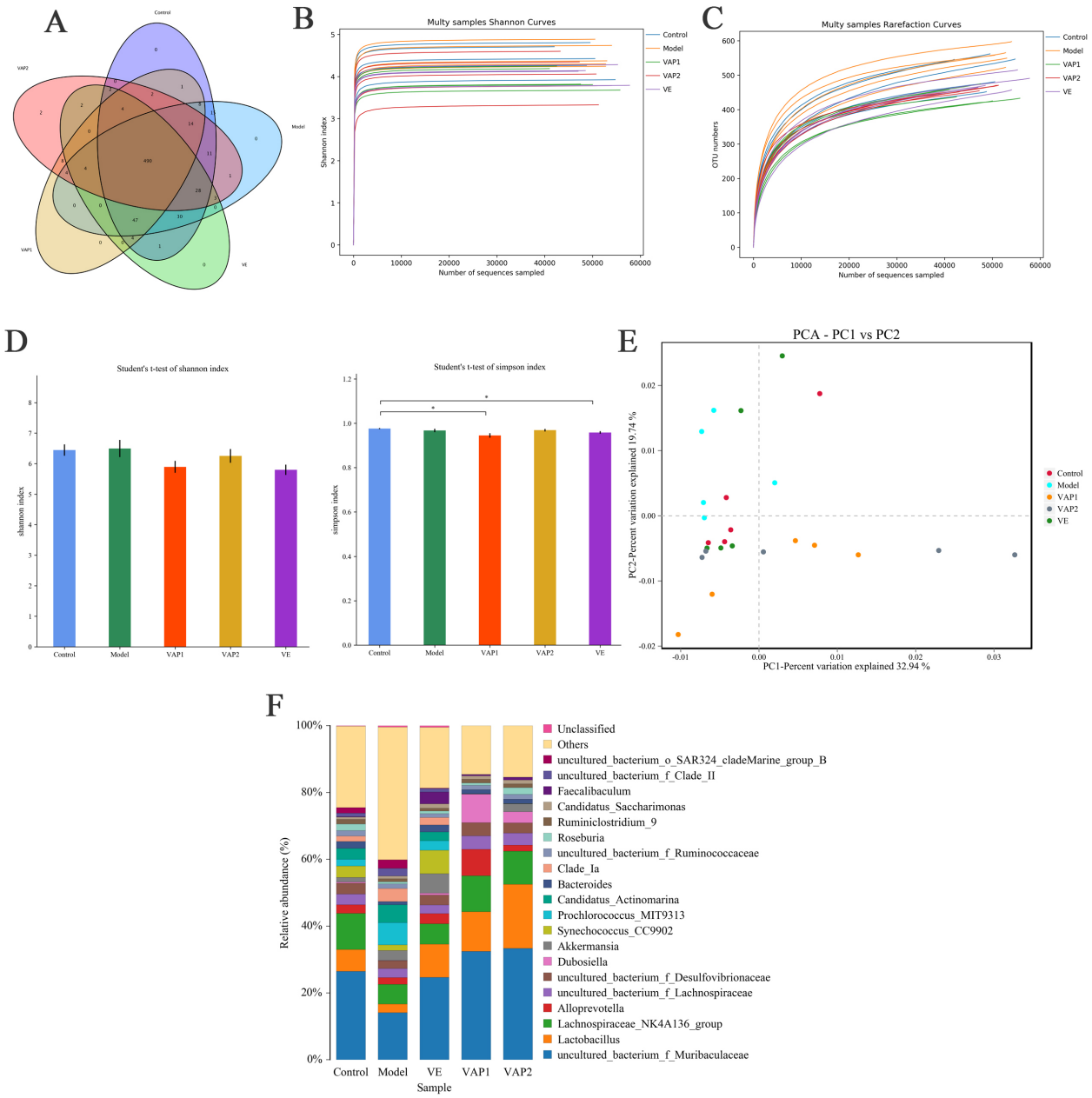

Fig. 4. Effects of VAP on the overall structure of the intestinal flora in aging mice (n = 5). (A) Venn diagram of OTUs. Each OTU represents a microbe. (B) Shannon curves. Each curve represents a sample, and each group is marked with a different color. (C) Rarefaction curves. The graphs show the rate of emergence of new OTUs under continuous sampling conditions. (D) Bacterial α-diversity estimated by the Shannon and Simpson indices $^*P < 0.05$. (E) Principal component analysis(PCA) of gut microorganisms in mice. (F) The relative abundance at the genus level is shown. The different genera are color-coded.

selected key enzymes involved in beta-fatty acid oxidation, such as ACOX1 and CPT1A and the key regulators PPARα and APOE4 for western blot analysis.

As shown in Fig. 6A,B, the protein expression levels of PPARα, ACOX1, and CPT1A in the model group were significantly lower than those in the control group ($P < 0.01$, $P < 0.05$). In contrast, compared to the model group, the protein expression levels of PPARα, ACOX1 and CPT1A in the VAP1 group were significantly higher ($P < 0.05$). Additionally, the protein expression levels of PPARα, ACOX1, and CPT1A were also significantly higher in the VAP2 group than in the model group ($P < 0.05$, $P < 0.01$). Furthermore, the APOE4 protein level in the model group was significantly upregulated compared to that observed in the control group ($P < 0.01$). However, the expression of APOE4 in the VE and VAP2 groups was significantly downregulated compared to that observed in the model group ($P < 0.05$). These results indicate that VAP can reduce APOE4 protein expression in mouse brain tissues.

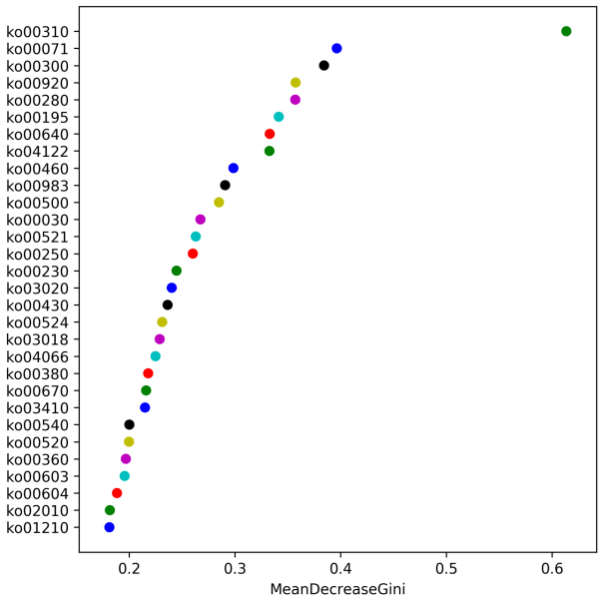

Fig. 5. 16S rRNA gene functional prediction analysis (n = 5). The greater the mean decrease in the Gini value is, the greater the influence of the pathway on the different groups. Each circle represents a pathway.

As shown in Fig. 6C, compared to the control group, FFA levels in the model group were significantly higher ($P < 0.01$). Compared to the model group, FFA levels in the VE, VAP1 and VAP2 groups were significantly lower ($P < 0.01$, $P < 0.05$). These results show that VAP reduced FFA levels in the brain tissue of aging mice, and the higher the dose was, the more obvious the effect.

The ATP content of mouse brain tissue was analyzed to determine the effect of VAP on ATP contents. As shown in Fig. 6D, the ATP content in the model group was significantly lower than that observed in the control group ($P < 0.01$). D-gal treatment reduced the ATP content in the brain tissue of mice. Compared to the model group, VAP and VE treatment significantly increased the ATP content in the brain tissue of mice ($P < 0.01$).

4. Discussion

Aging is marked by changes in the physiological functions of the brain. Brain aging is accompanied by learning and memory disorders [23], and the hippocampus plays a central role in the process of memory. The MWM test is one of the classic methods used to detect changes in ethology in learning and memory ability [24]. The behavioral results showed that D-gal-induced learning and memory disorders occurred in mice, with the behavior of mice demonstrating senescence-associated changes. Remarkably, the administration of VAP significantly improved the cognitive ability of aging mice. Moreover, H&E staining and TEM results revealed that the number of neurons in the model group decreased, and their morphology was abnormal. Altogether, these results suggest that VAP can protect the microstructure of neurons and improve cognitive impairment in D-gal-induced aging mice.

Aging is an inevitable stage in the process of life., during which the body experiences varying degrees of damage, leading to the occurrence of neurodegenerative diseases and the consequent impairment of learning and cognitive functions. The excessive accumulation of reactive oxygen species (ROS) is also closely associated with aging [25, 26]. Normally, ROS are involved in protein phosphorylation in various networks of the transport system. However, when ROS levels are excessive, lipid peroxidation occurs, resulting in oxidative damage [27, 28]. As important antioxidant enzymes in the body, SOD, CAT and GSH-Px protect cells from damage by scavenging free radicals [29]. SOD can catalyze the reduction of O^{2-} to hydrogen peroxide (H_2O_2), regulate the levels of ROS and reactive nitrogen clusters (RNS), and reduce cell damage [30]. CAT catalyzes the decomposition of H_2O_2 into water and oxygen, reduces the concentration of H_2O_2, accelerates the removal of O^{2-}, and reduces the damage of H_2O_2 to the body. As one of the products of the lipid peroxidation reaction of biomembranes, the concentration of MDA reflects the degree of damage to the body [31]. GSH-Px acts as a peroxide decomposing enzyme that reduces peroxide-induced cellular damage. The results showed that the activities of SOD, GSH-Px, CAT, and other antioxidant enzymes in the model group decreased. At the same time, the MDA content increased, which is consistent with the findings of previous studies [32]. We also observed that under VAP administration, the activities of antioxidant enzymes such as SOD, GSH-Px, and CAT in the serum tissues of mice were significantly improved, and the level of lipid peroxide MDA was significantly reduced. VAP is rich in antioxidant functional components [33] that can effectively remove free radicals and peroxides accumulated during the aging process, positively impacting the aging process.

The gut microbiota, also known as the "second genome", has been increasingly associated with human health [34]. Indeed, with the recent increase in the number of studies on this topic, the important role of the gut microbiota in the body has been widely recognized [35]. We combined behavioral experiments with high-throughput sequencing technology and observed that VAP administration significantly improved aging mice's learning and memory abilities. Analysis of the alpha diversity of the intestinal flora of mice in each group showed no significant difference in the alpha diversity of the intestinal flora of mice between the model group and each treatment group. PCA results showed that D-gal induced a large deviation in the type of flora in aging mice. The administration of VAP caused an increase in the similarity of the type of flora observed between aging and normal mice. For instance, at the genus level, VAP significantly increased the abundance of beneficial *Lactobacillus*. It is worth noting that *Lactobacillus* probiotics were demonstrated to protect cognitive function and improve lipid metabolism.

Based on the predicted functions of 16S rRNA gene functional genes, the KEGG analysis results [36] highlighted the

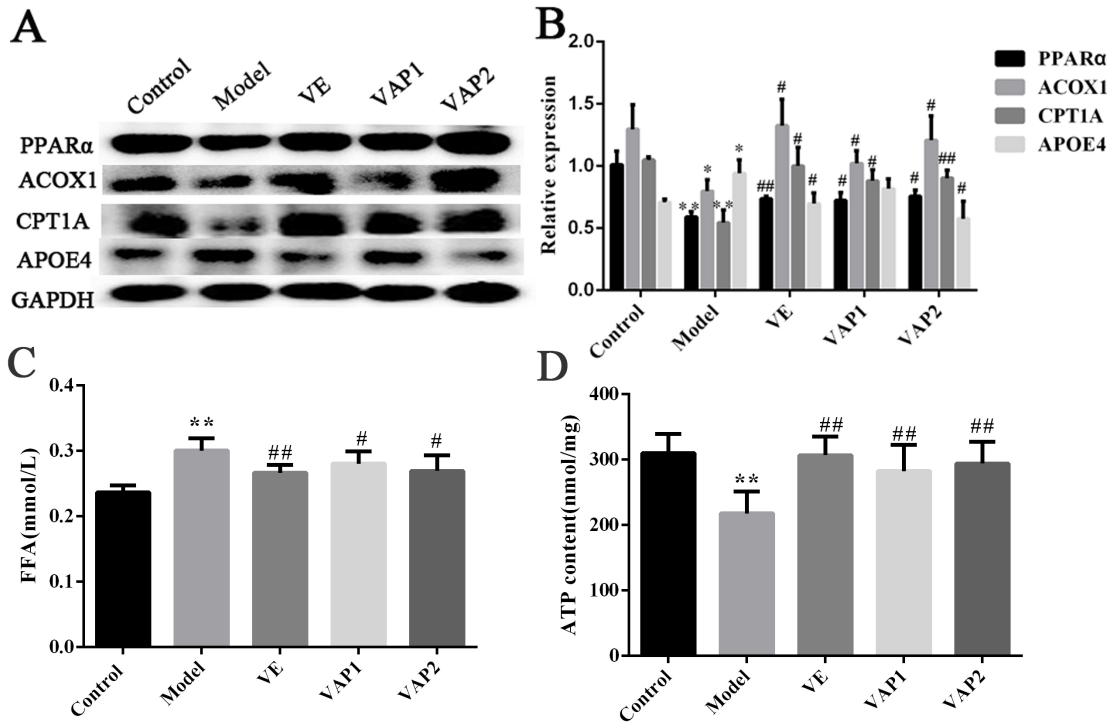

Fig. 6. Influence of VAP on fatty acid metabolism. (A,B) The expression of PPARα, ACOX1, CPT1A and APOE4 was assessed by western blotting (n = 3). (C) Detection of FFA levels in brain tissues (n = 8). (D) Detection of ATP contents in brain tissues (n = 8). Significant differences are denoted as follows: compared to the control group, $^{*}P < 0.05$, $^{**}P < 0.01$; compared to the model group,$^{\#}P < 0.05$,$^{\#\#}P < 0.01$.

fatty acid degradation pathway. We speculate that the aging caused by D-gal may be related to the abnormal metabolism of fatty acids in the body. Fatty acids are important structural components and energy sources of the body, and their content is affected by decomposition and synthesis rates [37]. As the brain is rich in lipids [38], this organ is particularly sensitive to OS due to its low free radical scavenging ability and weak antioxidant environment. Clinical studies have shown that the accumulation of extremely long-chain saturated fatty acids increases in patients with defects in peroxidase oxidase. At the same time, such patients suffer from impaired brain function and cognitive impairment [39]. Intestinal probiotics such as *Lactobacillus* help to regulate brain function and behavior [40]. Through neuroendocrine-immune system regulation, directly or indirectly mediates the microbial gut-brain axis, which has an important impact on the physiological function of the host [41, 42]. The gut-brain axis refers to the two-way signal mechanism between the gastrointestinal tract and the central nervous system. Related metabolites of intestinal microbes can effectively improve cognitive function by participating in oxidative stress and fatty acid metabolism [43, 44]. Therefore, VAP may play a role through the brain-gut axis by regulating the composition of the intestinal flora, reducing oxidative stress and fatty acid accumulation, promoting ATP energy supply, and ultimately improving cognitive impairment in aging mice.

The metabolism of fatty acids primarily occurs in the mitochondria and peroxisomes via β-oxidation. Mitochondria primarily break down short- and medium-to-long-chain fatty acids, while peroxisomes primarily break down long- and very-long-chain fatty acids. The result of fatty acid metabolism is the generation of ATP [45]. This experiment shows that after VAP regulates fatty acid metabolism in aging mice, it further increases the ATP content of aging mice and improves energy metabolism in aging mice [46, 47]. Although the mitochondrial and peroxisomal fatty acid oxidation decomposition products are the same, they are catalyzed by different enzymes. Importantly, senescence is known to reduce peroxisomal oxidation and the levels of ACOX1 [48]. ACOX1 acts as a rate-limiting enzyme that catalyzes the metabolism of straight-chain fatty acids and is involved in the synthesis of precursors of specific decomposition mediators (SPMs).

Interestingly, in neurodegenerative diseases, increased SPM content has been shown to effectively improve the survival rate of neurons and the pathogenesis of diseases [49]. CPT1A is located in the outer mitochondrial membrane and is also a key enzyme in the mitochondrial β-oxidation of fatty acids. Notably, both ACOX1 and CPT1A are regulated by PPARα, the activation of which upregulates the expression of these two key enzymes and accelerates fatty acid decomposition [50]. The main function of PPARα is to regulate fatty acid oxidation metabolism and energy consumption by regulating the activity of ACOX1 and CPT1A. We showed

that the administration of VAP induced the upregulation of the expression of PPARα, CPT1A, and ACOX1, suggesting that it may upregulate the expression of the latter two key enzymes via the activation of PPARα to promote fatty acid degradation.

APOE is the primary component of plasma lipoproteins and the most important carrier of cerebral cholesterol [51], playing a role in regulating lipid metabolism in the central nervous system and maintaining lipid metabolism balance in the brain [52]. Studies have shown that APOE can participate in the growth and repair of neurons, affect dendritic reconstruction and promote synapse generation via the regulation of lipid metabolism and possibly via the regulation of the cytoskeleton (e.g., affecting the phosphorylation of the tau protein) [53, 54]. These biological activities of APOE suggest that it may play an important role in nerve tissue repair [55]. APOE has three common isotypes (APOE2, APOE3, and APOE4), and studies have shown that APOE4 can lead to mitochondrial dysfunction in the brain. Indeed, the cerebral synapses in APOE4 gene carriers are severely damaged [56] and are more likely to suffer from neurodegenerative diseases [57]. Importantly, we showed that VAP could reduce the expression of APOE4 in the brain.

5. Conclusions

Results conclusively show that VAP promotes the expression of CPT1A and ACOX1 by activating PPARα, regulates the intestinal flora of aging mice, thereby improving lipid metabolism in aging mice, reducing fatty acid content, promoting fatty acid decomposition, and increasing ATP in aging mice. VAP increases ATP and reduces the expression of APOE by reducing fatty acid content in the brain of aging mice, thereby improving the cognitive impairment caused by aging, improving learning ability, and protecting neurons.

Abbreviations

VA, velvet antler; VAP, velvet antler polypeptide; D-gal, D-galactose; H&E, hematoxylin-eosin; TEM, transmission electron microscopy; SOD, superoxide dismutase; MDA, malonaldehyde; GSH-Px, glutathione peroxidase; CAT, catalase; CNS, central nervous system; OS, oxidative stress; ROS, reactive oxygen species; OTUs, operational taxonomic units; KEGG, Kyoto Encyclopedia of Genes and Genomes; PPARα, peroxisome proliferator-activated receptor α; CPT1A, carnitine-palmitoyl transferase-1 A; ACOXl, acyl-CoA oxidase 1; APOE4, apolipoprotein E4.

Author contributions

NL and QY conceived and designed the experiments; XRL, ZZ, STM, ZL, YXL, YHZ, QHP and SG performed the experiments; XCL, MK, JNL and JFW analyzed the data; HL contributed materials; XRL wrote the paper.

Ethics approval and consent to participate

All animal experiments performed in this study aligned with the relevant guidelines and were approved by the Laboratory Animal Ethics Committee at the Changchun University of Chinese Medicine (20180056).

Acknowledgment

We thank the anonymous reviewers for their excellent criticism of the article.

Funding

This study was supported by the National Key Research and Development Program of China (2018YFC1706603-05).

Conflict of interest

The authors declare no conflict of interest.

References

[1] Sui Z, Zhang L, Huo Y, Zhang Y. Bioactive components of velvet antlers and their pharmacological properties. Journal of Pharmaceutical and Biomedical Analysis. 2014; 87: 229–240.

[2] Ding Y, Ko S, Moon S, Lee S. Protective Effects of Novel Antioxidant Peptide Purified from Alcalase Hydrolysate of Velvet Antler Against Oxidative Stress in Chang Liver Cells *in Vitro* and in a Zebrafish Model *In Vivo*. International Journal of Molecular Sciences. 2019; 20: 5187.

[3] Tseng S, Sung C, Chen L, Lai Y, Chang W, Sung H, *et al.* Comparison of chemical compositions and osteoprotective effects of different sections of velvet antler. Journal of Ethnopharmacology. 2014; 151: 352–360.

[4] Zha E, Li X, Li D, Guo X, Gao S, Yue X. Immunomodulatory effects of a 3.2kDa polypeptide from velvet antler of Cervus nippon Temminck. International Immunopharmacology. 2013; 16: 210–213.

[5] Yang Q, Lin J, Sui X, Li H, Kan M, Wang J, *et al.* Antiapoptotic effects of velvet antler polypeptides on damaged neurons through the hypothalamic-pituitary-adrenal axis. Journal of Integrative Neuroscience. 2020; 19: 469.

[6] Cenini G, Lloret A, Cascella R. Oxidative Stress in Neurodegenerative Diseases: from a Mitochondrial Point of View. Oxidative Medicine and Cellular Longevity. 2019; 2019: 2105607.

[7] Chen P, Chen F, Zhou B. Antioxidative, anti-inflammatory and anti-apoptotic effects of ellagic acid in liver and brain of rats treated by D-galactose. Scientific Reports. 2018; 8: 1465.

[8] Su B, Wang X, Nunomura A, Moreira P, Lee H, Perry G, *et al.* Oxidative Stress Signaling in Alzheimer's Disease. Current Alzheimer Research. 2008; 5: 525–532.

[9] Rehman SU, Shah SA, Ali T, Chung JI, Kim MO. Anthocyanins Reversed D-Galactose-Induced Oxidative Stress and Neuroinflammation Mediated Cognitive Impairment in Adult Rats. Molecular Neurobiology. 2017; 54: 255–271.

[10] Feuerstein D, Backes H, Gramer M, Takagaki M, Gabel P, Kumagai T, *et al.* Regulation of cerebral metabolism during cortical spreading depression. Journal of Cerebral Blood Flow and Metabolism. 2016; 36: 1965–1977.

[11] Hébuterne X. Gut changes attributed to ageing: effects on intestinal microflora. Current Opinion in Clinical Nutrition and Metabolic Care. 2003; 6: 49–54.

[12] Sommer F, Bäckhed F. The gut microbiota–masters of host development and physiology. Nature Reviews. Microbiology. 2013; 11: 227–238.

[13] Lynch SV, Pedersen O. The Human Intestinal Microbiome in Health and Disease. New England Journal of Medicine. 2016; 375: 2369–2379.

[14] Cryan JF, O'Riordan KJ, Sandhu K, Peterson V, Dinan TG. The

gut microbiome in neurological disorders. Lancet Neurology. 2020; 19: 179–194.
[15] Kim S, Jazwinski SM. The Gut Microbiota and Healthy Aging: a Mini-Review. Gerontology. 2018; 64: 513–520.
[16] Hor Y, Ooi C, Khoo B, Choi S, Seeni A, Shamsuddin S, *et al.* Lactobacillus Strains Alleviated Aging Symptoms and Aging-Induced Metabolic Disorders in Aged Rats. Journal of Medicinal Food. 2019; 22: 1–13.
[17] Edgar RC. UPARSE: highly accurate OTU sequences from microbial amplicon reads. Nature Methods. 2013; 10: 996–998.
[18] Wang Y, Sheng H, He Y, Wu J, Jiang Y, Tam NF, *et al.* Comparison of the levels of bacterial diversity in freshwater, intertidal wetland, and marine sediments by using millions of illumina tags. Applied and Environmental Microbiology. 2013; 78: 8264–8271.
[19] Parks DH, Tyson GW, Hugenholtz P, Beiko RG. STAMP: statistical analysis of taxonomic and functional profiles. Bioinformatics. 2014; 30: 3123–3124.
[20] Hashimoto K, Goto S, Kawano S, Aoki-Kinoshita KF, Ueda N, Hamajima M, *et al.* KEGG as a glycome informatics resource. Glycobiology. 2006; 16: 63R–70R.
[21] Grice EA, Kong HH, Conlan S, Deming CB, Davis J, Young AC, *et al.* Topographical and Temporal Diversity of the Human Skin Microbiome. Science. 2009; 324: 1190–1192.
[22] Hor Y, Lew L, Jaafar MH, Lau AS, Ong J, Kato T, *et al.* Lactobacillus sp. improved microbiota and metabolite profiles of aging rats. Pharmacological Research. 2019; 146: 104312.
[23] Walker L, McAleese KE, Erskine D, Attems J. Neurodegenerative Diseases and Ageing. Subcellular Biochemistry. 2019; 18: 75–106.
[24] Lindner MD. Reliability, Distribution, and Validity of Age-Related Cognitive Deficits in the Morris Water Maze. Neurobiology of Learning and Memory. 1997; 68: 203–220.
[25] Puca AA, Carrizzo A, Villa F, Ferrario A, Casaburo M, Maciąg A, *et al.* Vascular ageing: the role of oxidative stress. International Journal of Biochemistry and Cell Biology. 2013; 45: 556–559.
[26] Maynard S, Fang EF, Scheibye-Knudsen M, Croteau DL, Bohr VA. DNA Damage, DNA Repair, Aging, and Neurodegeneration. Cold Spring Harbor Perspectives in Medicine. 2015; 5: a025130.
[27] Floyd RA, Hensley K. Oxidative stress in brain aging. Implications for therapeutics of neurodegenerative diseases. Neurobiology of Aging. 2003; 23: 795–807.
[28] Zorić L, Colak E, Canadanović V, Kosanović-Jaković N, Kisić B. Oxidation stress role in age-related cataractogenesis. Medicinski Pregled. 2010; 63: 522–526. (In Serbian)
[29] Inal ME, Kanbak G, Sunal E. Antioxidant enzyme activities and malondialdehyde levels related to aging. Clinica Chimica Acta. 2001; 305: 75–80.
[30] Wang Y, Branicky R, Noë A, Hekimi S. Superoxide dismutases: Dual roles in controlling ROS damage and regulating ROS signaling. Journal of Cell Biology. 2018; 217: 1915–1928.
[31] Sun J, Zhang L, Zhang J, Ran R, Shao Y, Li J, *et al.* Protective effects of ginsenoside Rg1 on splenocytes and thymocytes in an aging rat model induced by d-galactose. International Immunopharmacology. 2018; 58: 94–102.
[32] Ziegler DV, Wiley CD, Velarde MC. Mitochondrial effectors of cellular senescence: beyond the free radical theory of aging. Aging Cell. 2015; 14: 1–7.
[33] Zhu W, Wang H, Zhang W, Xu N, Xu J, Li Y, *et al.* Protective effects and plausible mechanisms of antler-velvet polypeptide against hydrogen peroxide induced injury in human umbilical vein endothelial cells. Canadian Journal of Physiology and Pharmacology. 2017; 95: 610–619.
[34] Cong X, Henderson WA, Graf J, McGrath JM. Early Life Experience and Gut Microbiome: the Brain-Gut-Microbiota Signaling System. Advances in Neonatal Care. 2015; 15: 314–323.
[35] Sudo N, Chida Y, Aiba Y, Sonoda J, Oyama N, Yu X, *et al.* Postnatal microbial colonization programs the hypothalamic-pituitary-adrenal system for stress response in mice. Journal of Physiology. 2004; 558: 263–275.
[36] Kanehisa M, Sato Y. KEGG Mapper for inferring cellular functions from protein sequences. Protein Science. 2020; 29: 28–35.
[37] Lang R, Mattner J. The role of lipids in host microbe interactions. Frontiers in Bioscience (Landmark Edition). 2017; 22: 1581–1598.
[38] Hu T, Zhu Q, Hu Y, Kamal G, Feng Y, Manyande A, *et al.* Qualitative and Quantitative Analysis of Regional Cerebral Free Fatty Acids in Rats Using the Stable Isotope Labeling Liquid Chromatography-Mass Spectrometry Method. Molecules. 2020; 25: 5163.
[39] Forman BM, Chen J, Evans RM. Hypolipidemic drugs, polyunsaturated fatty acids, and eicosanoids are ligands for peroxisome proliferator-activated receptors alpha and delta. Proceedings of the National Academy of Sciences of the United States of America. 1997; 94: 4312–4317.
[40] Sanborn V, Azcarate-Peril MA, Updegraff J, Manderino LM, Gunstad J. A randomized clinical trial examining the impact of LGG probiotic supplementation on psychological status in middle-aged and older adults. Contemporary Clinical Trials Communications. 2018; 12: 192–197.
[41] Hamidi N, Nozad A, Sheikhkanloui Milan H, Amani M. Okadaic acid attenuates short-term and long-term synaptic plasticity of hippocampal dentate gyrus neurons in rats. Neurobiology of Learning and Memory. 2019; 158: 24–31.
[42] Angelucci F, Cechova K, Amlerova J, Hort J. Antibiotics, gut microbiota, and Alzheimer's disease. Journal of Neuroinflammation. 2019; 16: 108.
[43] Hoffman BU, Lumpkin EA. A gut feeling. Science. 2018; 361: 1203–1204.
[44] Azad MAK, Sarker M, Li T, Yin J. Probiotic Species in the Modulation of Gut Microbiota: an Overview. BioMed Research International. 2018; 2018: 9478630.
[45] Thomas M, Davis T, Loos B, Sishi B, Huisamen B, Strijdom H, *et al.* Autophagy is essential for the maintenance of amino acids and ATP levels during acute amino acid starvation in MDAMB231 cells. Cell Biochemistry and Function. 2018; 36: 65–79.
[46] Pyper SR, Viswakarma N, Yu S, Reddy JK. PPARalpha: energy combustion, hypolipidemia, inflammation and cancer. Nuclear Receptor Signaling. 2010; 8: e002.
[47] Jin X, Xue B, Ahmed RZ, Ding G, Li Z. Fine particles cause the abnormality of cardiac ATP levels via PPARα-mediated utilization of fatty acid and glucose using *in vivo* and in vitro models. Environmental Pollution. 2019; 249: 286–294.
[48] Fransen M, Nordgren M, Wang B, Apanasets O, Van Veldhoven PP. Aging, age-related diseases and peroxisomes. Sub-Cellular Biochemistry. 2013; 69: 45–65.
[49] Vamecq J, Andreoletti P, El Kebbaj R, Saih F, Latruffe N, El Kebbaj MHS, *et al.* Peroxisomal Acyl-CoA Oxidase Type 1: Anti-Inflammatory and Anti-Aging Properties with a Special Emphasis on Studies with LPS and Argan Oil as a Model Transposable to Aging. Oxidative Medicine and Cellular Longevity. 2018; 2018: 6986984.
[50] Robertson G, Leclercq I, Farrell GC. Nonalcoholic steatosis and steatohepatitis. II. Cytochrome P-450 enzymes and oxidative stress. American Journal of Physiology—Gastrointestinal and Liver Physiology. 2001; 281: G1135–G1139.
[51] Boehm-Cagan A, Bar R, Harats D, Shaish A, Levkovitz H, Bielicki JK, *et al.* Differential Effects of apoE4 and Activation of ABCA1 on Brain and Plasma Lipoproteins. PLoS ONE. 2016; 11: e0166195.
[52] Nunes VS, Cazita PM, Catanozi S, Nakandakare ER, Quintão ECR. Decreased content, rate of synthesis and export of cholesterol in the brain of apoE knockout mice. Journal of Bioenergetics and Biomembranes. 2018; 50: 283–287.
[53] Rohn TT. Is apolipoprotein E4 an important risk factor for vascular dementia? International Journal of Clinical and Experimental Pathology. 2014; 7: 3504–3511.
[54] Zlokovic BV. Cerebrovascular effects of apolipoprotein E: implications for Alzheimer disease. JAMA Neurology. 2013; 70: 440–444.
[55] Serrano-Pozo A, Das S, Hyman BT. APOE and Alzheimer's disease: advances in genetics, pathophysiology, and therapeutic approaches. Lancet Neurology. 2021; 20: 68–80.
[56] Trojanowski JQ, Lee VMY. The role of tau in Alzheimer's disease. Medical Clinics of North America. 2002; 86: 615–627.
[57] Lin A, Parikh I, Yanckello L, White R, Hartz A, Taylor C, *et al.* APOE genotype-dependent pharmacogenetic responses to rapamycin for preventing Alzheimer's disease. Neurobiology of Disease. 2020; 139: 104834.